Research in Astron. Astrophys. **2012** Vol. **12** No. **8**, 973–994
http://www.raa-journal.org *http://www.iop.org/journals/raa*

***R**esearch in*
***A**stronomy and*
***A**strophysics*

X-ray spectroscopy of clusters of galaxies

Naomi Ota

Department of Physics, Nara Women's University, Kitauoyanishimachi, Nara, Nara 630-8506, Japan; *naomi@cc.nara-wu.ac.jp*

Received 2012 June 30; accepted 2012 July 8

Abstract Clusters of galaxies are the most massive objects in the Universe and precise knowledge of their mass structure is important to understand the history of structure formation and constrain still unknown types of dark contents of the Universe. X-ray spectroscopy of galaxy clusters provides rich information about the physical state of hot intracluster gas and the underlying potential structure. In this paper, starting from the basic description of clusters under equilibrium conditions, we review properties of clusters revealed primarily through X-ray observations considering their thermal and dynamical evolutions. The future prospects of cluster studies using upcoming X-ray missions are also mentioned.

Key words: galaxies: clusters: general — galaxies: intergalactic medium — X-rays: galaxies: clusters — cosmology: observations — cosmology: dark matter

1 INTRODUCTION

According to the standard cosmological model, the Universe began 13.8 billion years ago, and consists of 4% baryonic matter, 23% dark matter (of unknown type) and 73% dark energy (also of unknown origin) (Larson et al. 2011; Komatsu et al. 2011). Through interactions of these constituents, the associated cosmic structures have been evolving up to now. Our description of the Universe is often based on the notion that large objects, like galaxy clusters, that formed out of the evolving large-scale structure, have attained an equilibrium state in their matter and energy constituents. However, is this truly a natural assumption? To tackle this problem, focusing on objects appearing at the top of the hierarchical structure formation, namely clusters of galaxies, is vital in astrophysics.

Clusters of galaxies are the largest gravitationally bound systems in the Universe. This makes them very important probes of cosmology. Thus a precise knowledge of their mass structure is very important to measure the large-scale structure and to test cosmological models. In visible light, they are identified as groups of $\sim 100-1000$ galaxies, extending over $\sim 10^7$ light years (Fig. 1 left). On the other hand, X-ray observations of clusters have drastically changed our view of cosmic structure: hot gas fills inter-galactic space and emits strong X-rays (Fig. 1 right). Furthermore, the total mass of hot gas exceeds the sum of galaxy mass by two–three times. To confine the hot gas by gravitational forces, invisible matter, "dark matter," of five times larger mass is required. As techniques in X-ray spectroscopy and imaging observations have progressed, the presence of a complex temperature structure was also found in the X-ray emitting gas. Those facts have revealed that clusters preserve the past history of being built through complex interactions, particularly merging, between smaller systems. Thus the clusters are no longer thought to be in an equilibrium state, but rather dynamically evolving on cosmological time scales.

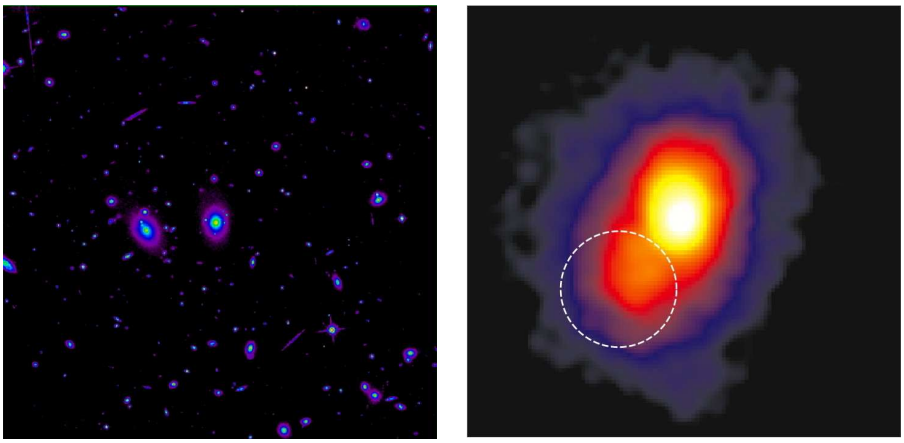

Fig. 1 Optical (*left*) and X-ray (*right*) images of a cluster of galaxies, RX J1347.5–1145, taken with the Hubble Space Telescope (the Multi-mission Archive at STScI) and the *Chandra* satellite respectively. In both panels, a side of the figure is $110''$, corresponding to about 630 kpc. The white circle in the right panel indicates a location where extremely hot thermal gas has been discovered (see Sect. 4.3).

This paper is organized as follows: in Section 2 a general description of clusters is summarized. In Sections 3–4, properties of clusters of galaxies revealed primarily by X-ray observations are reviewed in light of their thermal and dynamical evolutions. Finally in Section 5, future prospects are briefly mentioned. We use $\Omega_M = 0.3$, $\Omega_\Lambda = 0.7$ and $h_{70} \equiv H_0/(70\ \mathrm{km\,s^{-1}\,Mpc^{-1}}) = 1$ throughout the paper except where noted.

2 SPATIAL DISTRIBUTION OF MATTER AND X-RAY EMISSION

In the X-ray energy band, clusters of galaxies look very different from the optical view; hot diffuse plasma with a temperature of $\sim 10^7 - 10^8$ K fills the intracluster space. The X-ray emitting hot plasma is confined in the cluster's gravitational potential and is believed to trace the underlying dark matter distribution. The typical X-ray luminosity of clusters is $10^{44} \sim 10^{45}\ \mathrm{erg\,s^{-1}}$, and the electron number density of hot plasma at the center of clusters is typically $10^{-3} \sim 10^{-2}\,\mathrm{cm^{-3}}$. In what follows, the general view of clusters of galaxies under equilibrium models is summarized.

2.1 Hydrostatic Equilibrium Condition and the β-model

Since the collision time scales for ions and electrons in the intracluster gas are much shorter than the time scales of heating or cooling, we can treat the gas as a fluid (Sarazin 1988). In general, the sound crossing time t_s, i.e., the time required for a sound wave in the intracluster gas to cross a cluster with radius R,

$$t_\mathrm{s} \equiv \frac{2R}{c_\mathrm{s}} \sim 2\ \mathrm{Gyr} \left(\frac{R}{1\ \mathrm{Mpc}}\right) \left(\frac{c_\mathrm{s}}{1000\ \mathrm{km\,s^{-1}}}\right)^{-1} \tag{1}$$

is shorter than the probable age of the cluster or the Hubble time, $t_\mathrm{H} = H_0^{-1} \sim 14\,\mathrm{Gyr}$. Thus the gas is considered to be in hydrostatic equilibrium. In addition, if the cluster is spherically distributed, the hydrostatic equation reads

$$\frac{1}{\rho_\mathrm{g}} \frac{dP_\mathrm{g}}{dr} = -\frac{d\phi}{dr} = -\frac{GM(r)}{r^2}\,, \tag{2}$$

where $M(r)$ is the total cluster mass (i.e., dark matter + galaxies + hot gas) within the radius r and $P_{\rm g}$ is the thermal pressure and a product of gas density and temperature, $n_{\rm g}(r)kT_{\rm g}(r)$. If the self-gravity of the gas is ignored, the distribution of gas is determined by the cluster potential, ϕ.

A temperature gradient in the plasma is smoothed by heat conduction. If the heat conduction were sufficiently rapid compared to other important time scales, the gas would become isothermal. Substituting the gas pressure $P(r) = n_{\rm g}(r)T_{\rm g}$ into Equation (1) and assuming $T_{\rm g}$ is constant, we obtain

$$\frac{d\ln\rho_{\rm g}}{dr} = -\frac{\mu m_p}{kT_{\rm g}}\frac{d\phi}{dr}\,, \tag{3}$$

where μ is the mean molecular weight, ~ 0.6. Similarly, the galaxies are bounded in the gravitational potential, whose hydrostatic condition is written as

$$\frac{d\ln\rho_{\rm G}}{dr} = -\frac{1}{\sigma^2}\frac{d\phi}{dr}\,. \tag{4}$$

σ is the line-of-sight velocity dispersion and is typically of the order of 1000 $\mathrm{km\,s^{-1}}$. From Equations (2) and (3), we find

$$\rho_{\rm g} = \rho_{\rm G}^{\beta}, \qquad \beta \equiv \frac{\mu m_p \sigma^2}{kT_{\rm g}}\,. \tag{5}$$

Hence the gas distribution differs just by the index β in comparison with that of member galaxies.

King (1962) derived an analytic approximation to the isothermal sphere of self-gravitational isothermal collision-less particles. The density profile of the cluster's member galaxies has been found to be well approximated by the King profile,

$$\rho_{\rm G} \sim \rho_{\rm King} = \rho_0 \left[1 + \left(\frac{r}{r_{\rm c}}\right)^2\right]^{-3/2}\,. \tag{6}$$

Here $r_{\rm c}$ represents a core radius within which the density is regarded as constant. From Equations (4) and (5), the isothermal gas distribution is represented by

$$\rho_{\rm g} = \rho_{\rm g0} \left[1 + \left(\frac{r}{r_{\rm c}}\right)^2\right]^{-3\beta/2}\,. \tag{7}$$

This formula is called the isothermal β-model (Cavaliere & Fusco-Femiano 1976).

2.2 X-ray Emission Process

An X-ray spectrum emitted from an ionized intracluster plasma is described with a combination of continuum emission and line emission from heavy elements. The former is produced by free-free (or bremsstrahlung), free-bound, two-photon emission and the latter by one-electron radiative transitions, dielectric recombination satellite lines, and inner-shell ionization (van Paradijs & Bleeker 1999; Böhringer & Werner 2010).

In the temperature range of clusters ($kT > 2$ keV), the total emission is dominated by the free-free emission if the abundance of heavy elements does not exceed the solar abundance by very much. The emissivity of the free-free emission at a frequency ν from a hot plasma with an electron temperature of $T_{\rm g}$ is given by

$$\epsilon_\nu^{\rm ff} = \frac{2^5\pi e^6}{3m_{\rm e}c^3}\Big(\frac{2\pi}{2m_{\rm e}k}\Big)^{1/2} n_{\rm e}\sum Z^2 n_{\rm i} g_{\rm ff}(Z,T_{\rm g},\nu)\times T_{\rm g}^{-1/2}\exp\left(-h\nu/kT_{\rm g}\right) \tag{8}$$

$$= \Lambda(T,Z,\nu)n_{\rm e}^2\,, \tag{9}$$

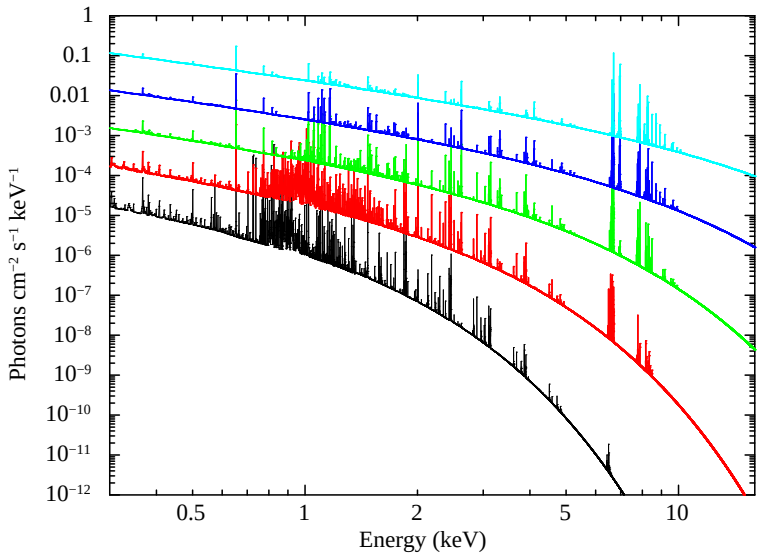

Fig. 2 APEC thin-thermal plasma model for $kT/[\mathrm{keV}] = 1$ (*black*), 2 (*red*), 4 (*green*), 8 (*blue*), 16 (*cyan*), and the metal abundance of 0.3 solar. The graphs are shifted in the y-direction for clarity.

where Z is the charge of an ion in a plasma; n_i and n_e are the number density of ions and electrons, respectively (e.g., Rybicki & Lightman 1985). The Gaunt factor is a correction factor for quantum mechanical effects and is approximately $g_\mathrm{ff} \sim 0.9(h\nu/kT)^{-0.3}$. The bolometric emissivity is then

$$\begin{aligned} \epsilon^\mathrm{ff} &= \int_0^\infty \epsilon_\nu^\mathrm{ff} d\nu = \Lambda(T,Z) n_\mathrm{e}^2 \\ &\sim 1.435 \times 10^{-27} \bar{g} T_\mathrm{g}^{1/2} n_\mathrm{e} \sum Z^2 n_\mathrm{i} \, [\mathrm{erg\ s^{-1}\ cm^{-3}}] \, . \end{aligned} \tag{10}$$

Precise X-ray emission spectra from thin-thermal plasma can be calculated by utilizing plasma codes such as APEC (Smith et al. 2001) and MEKAL (Mewe et al. 1985, 1986; Kaastra 1992; Liedahl et al. 1995). The updated version of the latter is available in the SPEX package (Kaastra et al. 1996). For reference, the APEC models for various temperatures are plotted in Figure 2. The metal abundance is assumed to be 0.3 solar, as is typical of intracluster gas (Mushotzky & Loewenstein 1997). The abundance table of Anders & Grevesse (1989) is used here[1].

2.3 β-profile and Hydrostatic Mass Estimate

The surface brightness profile of an isothermal spherical plasma with a radial density profile given by Equation (7) is calculated by integrating the local emission per unit volume (Eq. (10)) and the density along the line of sight. We obtain the X-ray surface brightness $S(r)$ at a projected radius r,

$$S(r) = S_0 \left[1 + \left(\frac{r}{r_\mathrm{c}} \right)^2 \right]^{-3\beta+1/2} , \tag{11}$$

$$S_0 \equiv n_{\mathrm{e}0} n_{\mathrm{H}0} \Lambda(T,Z) \frac{\sqrt{\pi} r_\mathrm{c}}{4\pi D_\mathrm{L}^2} \frac{\Gamma(3\beta - 1/2)}{\Gamma(3\beta)} \, [\mathrm{erg\ s^{-1}\ cm^{-4}}] \, . \tag{12}$$

[1] The updated table for the solar system abundance is given in Lodders (2003).

Here n_{e0} and $n_{\rm H0}$ are the central electron and hydrogen densities of the intracluster gas respectively and $D_{\rm L}$ is a luminosity distance to the object. It is known that the observed cluster's X-ray surface brightness is well fitted with the above function, and $\beta \sim 0.6-0.7$ on average (e.g., Jones & Forman 1984; Ota & Mitsuda 2004).

Once we have obtained the β profile parameters to characterize the surface brightness distribution, we can estimate the three-dimensional density profile of the gas, i.e. the β-model. Then the mass of the gas inside a radius r is given by integrating Equation (7).

$$M_{\rm gas}(r) = 4\pi\rho_{\rm gas}(0){r_{\rm c}}^3 \int_0^x (1+x^2)^{-3\beta/2}x^2 dx\,, \tag{13}$$

where $x = r/r_{\rm c}$. From the assumption of hydrostatic equilibrium, we derive the total mass of the cluster inside a radius r,

$$M(r) = \frac{3kT\beta r}{\mu m_p G}\frac{(r/r_{\rm c})^2}{1+(r/r_{\rm c})^2}\,. \tag{14}$$

If gas is not isothermal and its temperature distribution has a radial dependence, $T_{\rm g}(r)$, the hydrostatic mass is rewritten as

$$M(r) = -\frac{kT_{\rm g}(r)r}{G\mu m_p}\left[\frac{\partial \ln n_{\rm g}(r)}{d\ln r} + \frac{\partial \ln T_{\rm g}(r)}{\partial \ln r}\right]\,. \tag{15}$$

As an illustration, the result of hydrostatic mass estimation under the isothermal β-model for a gravitational lensing cluster CL0024+17 ($z = 0.395$) is shown in Figure 3 and compared with an independent mass determination based on the gravitational lensing effect (Tyson et al. 1998). Since the lensing effect directly maps the surface mass density of the cluster, regardless of the internal dynamical and thermal state of the cluster, comparison of the two methods provides information on the physical state of clusters (Hattori et al. 1999; Kneib & Natarajan 2011, for review). In the case of CL0024+17, a factor of two–three discrepancy has been found between the hydrostatic and strong lensing mass estimates, indicating that the system is experiencing a line-of-sight merger (Ota et al. 2004; Zhang et al. 2005; Jee et al. 2007; Zu Hone et al. 2009).

2.4 Universal Dark Matter Density Profile

Navarro et al. (1997) found from their numerical simulations of structure formations under the Cold Dark Matter (CDM) model, that the collapsed dark matter halos with masses over several orders of magnitude follow a universal density profile,

$$\rho_{\rm NFW}(r) = \frac{\rho_s}{(r/r_s)(1+r/r_s)^2}\,, \tag{16}$$

where ρ_s and r_s are the characteristic density and length, respectively. ρ_s is related to the critical density of the universe $\rho_{\rm crit}$ and the characteristic density $\delta_{\rm c}$ through $\rho_s = \delta_{\rm c}\rho_{\rm crit}$. Instead of the flat core of the King profile, the NFW profile has a core with $\propto r^{-1}$ dependence. Although the density diverges at the center, the mass inside a radius r,

$$M_{\rm NFW}(r) = 4\pi\rho_s {r_s}^3\left[\ln(1+x) - \frac{x}{1+x}\right], \qquad x \equiv r/r_s\,, \tag{17}$$

converges to 0 as $r \to 0$.

The density distribution of intracluster gas in hydrostatic equilibrium with the NFW dark matter potential was analytically derived by Makino et al. (1998) assuming the masses of gas and galaxies are negligibly small compared to the dark matter.

$$\rho_{\rm gas}(r) \;=\; \rho_{\rm gas0}\exp\left[-B\left(1-\frac{\ln(1+x)}{x}\right)\right], \qquad B \equiv \frac{4\pi G\mu m_p \rho_s r_s^2}{kT}\,. \tag{18}$$

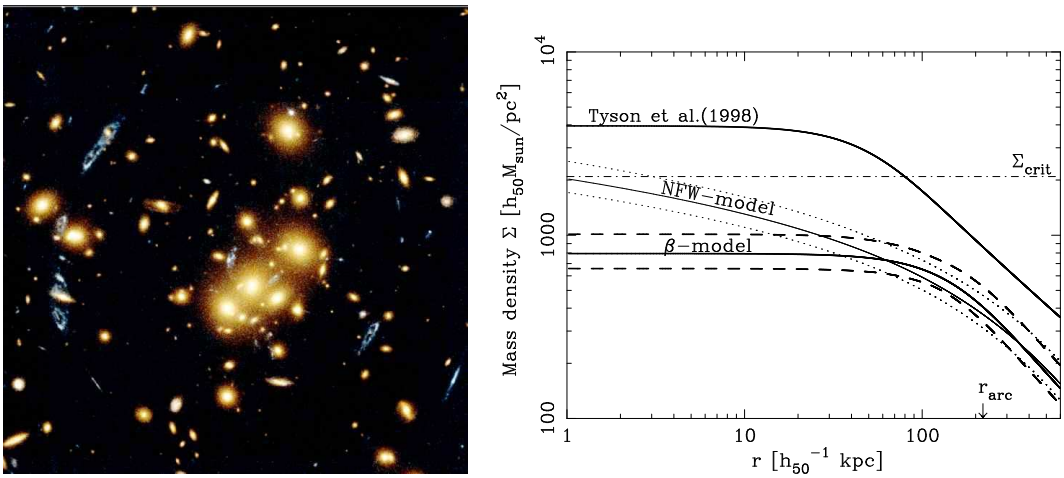

Fig. 3 HST/WFPC2 image of a lensing cluster with multiple lens arcs, CL0024+17 (*left*; W. N. Colley and E. Turner (Princeton University), J. A. Tyson (Bell Labs, Lucent Technologies) and NASA *http://hubblesite.org/newscenter/archive/releases/1996/10/image/a/*). Mass density profiles for the β-model and the NFW-model of the CL0024+17 main cluster (Ota et al. 2004) are shown and compared with the lensing mass model by Tyson et al. (1998) (*right*).

Then the mass of the gas within a radius r is given by

$$M_{\rm gas}(r) = 4\pi\rho_{\rm gas}(0)e^{-B}r_s^3\int_0^x x^2(1+x)^{B/x}dx\,. \tag{19}$$

Suto et al. (1998) generalized the universal density profile to the form $\rho \propto 1/[x^\mu(1+x^\nu)]^\lambda$ and numerically computed the gas density profile in hydrostatic equilibrium for the case of $\mu = \alpha$, $\nu = 1$, and $\lambda = 3-\alpha$ with the restriction $1 < \alpha < 2$. Note that the case with $\alpha = 1$, $\nu = 1$, and $\lambda = 2$ corresponds to the NFW model. They further computed the X-ray surface brightness distribution at a projected radius r on the sky, and derived a useful fitting formula in the following generalized shape.

$$\begin{aligned} S(r) &\propto \left[1+\left(\frac{r}{r_s\phi_{\rm c}}\right)^\zeta\right]^{-\eta}\,, \\ \phi_{\rm c} &= 0.3(2/\alpha-1)\,, \\ \zeta &= 0.41-5.4(2-\alpha)^6+(0.585+6.47\alpha^{-5.1B})B^{-\alpha^6/30}\,, \\ \eta &= -0.68-5.09(\alpha-1)^2+(0.202+0.0206\alpha^8)B^{1.1}\,. \end{aligned} \tag{20}$$

These expressions are valid for $5 \le B \le 20$ and $1.0 \le \alpha \le 1.6$ in the range $10^{-4} \le \phi \le \phi_{\rm max}$, where $S(\phi_{\rm max}) = 10^{-4}S(0)$. We refer to the formula with $\alpha = 1$ as the SSM model hereafter.

The SSM model has a surface brightness distribution similar to the β profile over a wide range of r, although it has an excess over the β-profile in the central region because of the strong concentration of the dark matter halo of the NFW model. Makino et al. (1998) fitted simulated gas profiles which obey the universal dark matter profile with the β-profile function, and noted that the best-fit relation between the scale parameter and the β-model core radius is given by $r_{\rm c} = 0.22\,r_s$.

Two kinds of density profiles, the β-model and the SSM model, have been introduced so far since they give reasonable approximations to observed gas profiles in studying the global cluster

structure. Deviation from those models sometimes seen at the center of clusters will be mentioned later.

2.5 Formation of Clusters and the Virial Radius

Numerical simulations based on the CDM model predict hierarchical structure formation, so rather continuous accretion of matter and sub-cluster merging occur in the process of cluster formation (e.g., Moore et al. 2001). Hence clusters reside at junctions of cosmic filaments and are connected to the surrounding filamentary structures. It is, however, practically important to define a 'cluster' based on some simple model. In this section we briefly review the collapse scenario according to the spherical collapse model (Gunn & Gott 1972). This model predicts a very important physical quantity of clusters, the virial radius.

At some time epoch, a certain region of the Universe which happens to have a higher mass density than the background due to fluctuations starts breaking away from the general expansion, and eventually collapses to form a cluster of galaxies. Since at the collapse epoch, $\Omega \sim 1$, we can neglect the Λ term in the equation of motion of the shell. We also assume that the amplitude of the density perturbation is small, i.e. $\delta \ll 1$. Then we have

$$\frac{d^2r}{dt^2} = -\frac{\mathrm{G}M}{r^2}\,, \tag{21}$$

where M is the mass inside the shell and is constant. The first integral of this equation is

$$\left(\frac{dr}{dt}\right)^2 = \frac{2\mathrm{G}M}{r} + C\,. \tag{22}$$

C is a constant, and the total energy $C/2$ must be negative for collapse to occur. The solution of Equation (22) is given in a parametric form,

$$t = \frac{\mathrm{G}M}{|C|^{3/2}}(\theta - \sin\theta), \qquad r = \frac{\mathrm{G}M}{|C|}(1 - \cos\theta)\,. \tag{23}$$

The radius, r, is 0 at $\theta = 0$, i.e. $t = 0$. Then it increases with increasing θ and takes the maximum value, $r_\mathrm{m} = 2\mathrm{G}M/|C|$ at $\theta = \pi$, i.e., $t = t_\mathrm{m} \equiv \pi\mathrm{G}M/|C|^{3/2}$ (turn around). Then it shrinks to 0 again at $\theta = 2\pi$, i.e., $t = t_\mathrm{c} \equiv 2\pi\mathrm{G}M/|C|^{3/2}$ (collapse). After collapse, the system will be virialized. In the virialized system, the potential energy is related to the total energy as $W = 2E$. Assuming the radius of the system after virialization is r_vir, we have

$$W = -\frac{\mathrm{G}M^2}{r_\mathrm{vir}} = 2E = -2\frac{\mathrm{G}M^2}{r_\mathrm{m}}\,. \tag{24}$$

Therefore, $r_\mathrm{vir} = r_\mathrm{m}/2$. The average density inside the virial radius r_vir is

$$\bar{\rho}_\mathrm{vir} = \frac{3}{4\pi}\frac{|C|^3}{\mathrm{G}^3M^2}\,. \tag{25}$$

On the other hand, the solution of Equation (22) with $C = 0$ describes the background expansion, because $\Omega \sim 1$. The solution is

$$r_\mathrm{b} = \left(\frac{9}{2}\mathrm{G}M\right)^{1/3} t^{2/3}\,. \tag{26}$$

The density inside r_b gives the critical density at t,

$$\rho_\mathrm{crit}(t = t_\mathrm{c}) = \frac{1}{24\pi^3}\frac{|C|^3}{G^3M^2}\,. \tag{27}$$

Thus we obtain the important relation,

$$\Delta_{\rm c} \equiv \frac{\bar{\rho}_{\rm vir}}{\rho_{\rm crit}} = 18\pi^2 \,. \tag{28}$$

We can assume that a cluster is virialized within the overdensity radius r_Δ at which the average density is equal to $\Delta_{\rm c}$ times the critical density of the collapsed epoch.

The spherical collapse in an $\Omega + \Lambda = 1$ Universe is presented in the Appendix of Nakamura & Suto (1997): a fitting formula for the overdensity in the flat Universe with finite Λ is

$$\Delta_{\rm c} \simeq 18\pi^2 \Omega^{0.437} \,. \tag{29}$$

By taking $\Delta_{\rm c} = 180$ or 200, the overdensity radius of r_{180} or r_{200} is often quoted as a measure of the cluster's virial radius. r_{500} is also frequently used for the reason that there is an indication from numerical simulation that the hydrostatic assumption is valid within that radius (Evrard et al. 1996) as well as that X-ray signals being detected out to r_{500} or roughly ~ 1 Mpc in many clusters (beyond that deeper exposure is required to trace emission from the tenuous matter). The temperature scaling for the overdensity radii for various Δ is derived using a nearby X-ray cluster sample (Arnaud et al. 2005): for $\Delta_{\rm c} = 500$, it resulted in $r_{500} h(z) = (1104 \pm 13)(kT/5\ {\rm keV})^{0.57\pm0.02}$ kpc.

2.6 Radiative Cooling of Gas

Since hot intracluster gas loses its thermal energy via X-ray emission, radiative cooling may affect the cluster structure once the gas is settled in the cluster's potential.

The thermal energy loss is expressed by

$$\frac{dE_{\rm e}}{dt} = -\epsilon^{\rm ff} \,, \tag{30}$$

where $E_{\rm e}$ is the thermal energy of electrons per unit volume and $E_{\rm e} = 3 n_{\rm e} k T_{\rm g}/2$. The volume emissivity, $\epsilon^{\rm ff}$, can be denoted as $\epsilon^{\rm ff} = q_{\rm ff} n_{\rm e}^2 T_{\rm g}^{1/2}$. Thus if the hot gas cools, keeping the density constant, the temperature decreases according to the following equation

$$\frac{dT_{\rm g}}{dt} = -a T_{\rm g}^{1/2}, \qquad a = \frac{2 q_{\rm ff} n_{\rm e}}{3k} \,. \tag{31}$$

The solution is

$$T_{\rm g}(t)^{1/2} = T_{\rm g}(0)^{1/2} - \frac{a}{2} t \,. \tag{32}$$

Thus the hot gas cools on the time scale

$$t_{\rm cool} = \frac{2 T_{\rm g}(0)^{1/2}}{a} = \frac{3 k T_{\rm g}(0)^{1/2}}{q_{\rm ff} n_e} \tag{33}$$

$$\sim 3 \times 10^9\ {\rm yr} \left(\frac{T_{\rm g}(0)}{4\ {\rm keV}} \right)^{1/2} \left(\frac{n_{\rm e}}{2 \times 10^{-2}\ {\rm cm}^{-3}} \right)^{-1} \,. \tag{34}$$

The cooling time scale for the central region of typical relaxed clusters is estimated to be shorter than the Hubble time, and the cluster core may be subject to radiative cooling. On the other hand, radiative cooling is not considered to be important outside the core region because of lower density.

3 THERMAL EVOLUTION OF INTRACLUSTER GAS

3.1 Cooling Problem

According to Section 2.6, gas at the cluster's center can radiate an amount of energy comparable to its total thermal energy in less than the Hubble time and thus cools. It was suggested from earlier works that the "cooling-flow" phenomenon would occur if the gas cools isobarically and no heating process balances this cooling, so the gas flows inward maintaining the thermal pressure (Fabian 1994). On the other hand, high-resolution X-ray spectroscopy showed that the temperature drops in the cooling cores by only a factor of two–three, and there is much less emission at low temperature, as predicted by the standard cooling-flow model (e.g., Kaastra et al. 2004). This observational finding triggered explorations into a variety of scenarios for gas heating: heat conduction, active galactic nucleus (AGN) heating, magnetic reconnections, cosmic-ray heating etc. X-ray and radio observations have provided evidence for the interaction of AGN jets with cluster gas (e.g., McNamara et al. 2000). Although the work done by uplifting AGN bubbles on the surrounding gas may be of the order of magnitude to compensate the radiation loss, how the feedback achieves a tuning between cooling and heating is not clear. The similarity and smoothness of cooling profiles indicate the need for a continuous, distributed heat source (for review, e.g., Peterson & Fabian 2006).

3.2 Statistical Properties of Cluster Cores

Regarding the density profile, a deviation from the conventional isothermal β-model is commonly seen at the center of clusters having a compact core (often termed Cool Core (CC) clusters): they exhibit systematically higher central density while the profiles are fairly universal outside $0.1r_{500} \sim 100$ kpc (Neumann & Arnaud 1999).

Figure 4 shows the gas density profiles derived with the single-β model (Ota et al. 2006). The density scatter is prominent within $\sim 0.1r_{500}$ and is found to be a significant source of scatter in the X-ray luminosity-temperature correlation (Ota et al. 2006; O'Hara et al. 2006; Chen et al. 2007).

The statistical properties of gas density structure have been investigated from systematic analysis of cluster samples by many authors (e.g., O'Hara et al. 2006; Ota et al. 2006; Chen et al. 2007; Santos et al. 2008; Cavagnolo et al. 2009; Hudson et al. 2010). These X-ray studies show that the fraction of CC clusters is roughly 50%. The rest of the sample without the central cool emission is called Non-Cool Core (NCC) clusters. Ota & Mitsuda (2002, 2004) first pointed out from the analysis of *ROSAT* and *ASCA* archival data that the histogram of the cluster core radius exhibits a high concentration around 50 and 200 h_{70}^{-1} kpc (Fig. 5). Later, a similar double-peaked distribution of core radius was shown independently by Hudson et al. (2010): they utilized the *Chandra* data set on a nearby flux-limited sample with higher resolution. The consistency between the two results gives a confirmation of this nature.

The relaxed clusters often host a central dominant elliptical galaxy, also called a cD galaxy, which deepens the cluster's potential well and causes a peaked gas profile (Ikebe et al. 1999). The regular clusters with a small core tend to contain a cD galaxy, however, not all of them have one. Thus it is unlikely that the small core represents the potential distribution of the cD galaxy itself (Akahori & Masai 2005).

Under the self-similar model, the internal structure of the gas should be scaled by the virial radius, and then $r_{500}/r_{\rm c}$ should be constant for all clusters. However, $r_{\rm c}$ does not simply scale by r_{500} (Fig. 5), particularly for those having a small core radius ($r_{\rm c} < 100$ kpc). This clear departure from the self-similar relation for small-core clusters suggests that the formation of the small cores is determined by some physical process other than the self-similar collapse.

An investigation of X-ray fundamental plane gives another clue to explore the evolution of clusters. The presence of a planer distribution of nearby clusters in 3-dimensional parameter space (the central gas density n_{r0}, core radius $r_{\rm c}$, and temperature T) was first noted by Fujita & Takahara

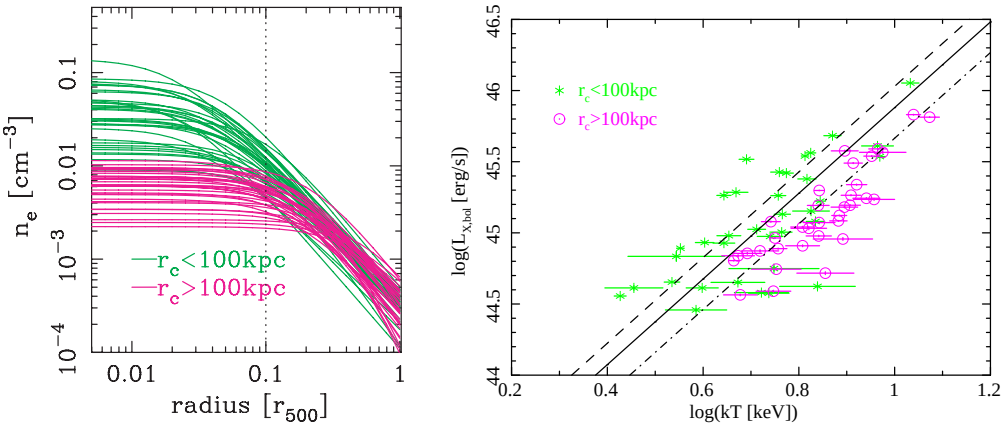

Fig. 4 (*Left*) Electron density profiles for 69 clusters. The best-fit density profiles derived with the single β-model are plotted, where the radius is normalized with r_{500}. $0.1r_{500}$ is indicated with the vertical dotted line, inside which the scatter is the most prominent. (*Right*) $L_X - T$ relation of clusters. A significant offset in the normalization factor of the $L_X - T$ relation between clusters with small ($r_c < 100$ kpc) and large core radii (> 100 kpc) is seen (Ota et al. 2006).

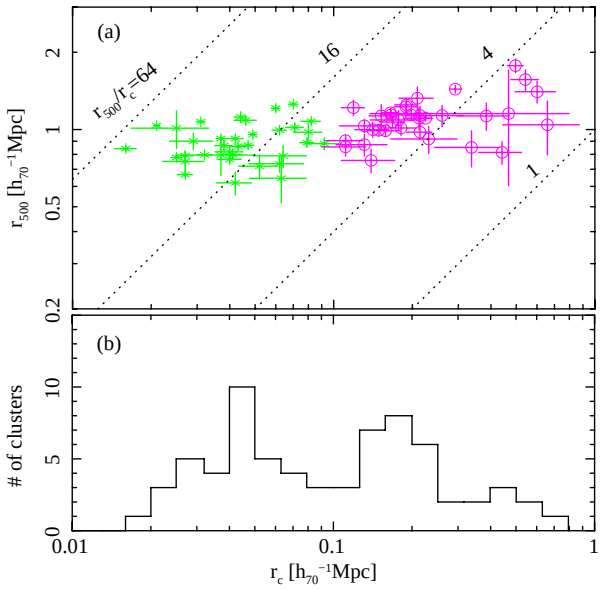

Fig. 5 (a) $r_{500} - r_c$ relation and (b) histogram of r_c for 69 clusters at $z > 0.1$. In panel (a), 35 clusters with a small core of $r_c < 100$ kpc and 34 clusters with a larger core of $r_c > 100$ kpc are shown with the asterisks and the circles, respectively. The dotted lines indicate the self-similar condition corresponding to four different constant values of r_{500}/r_c.

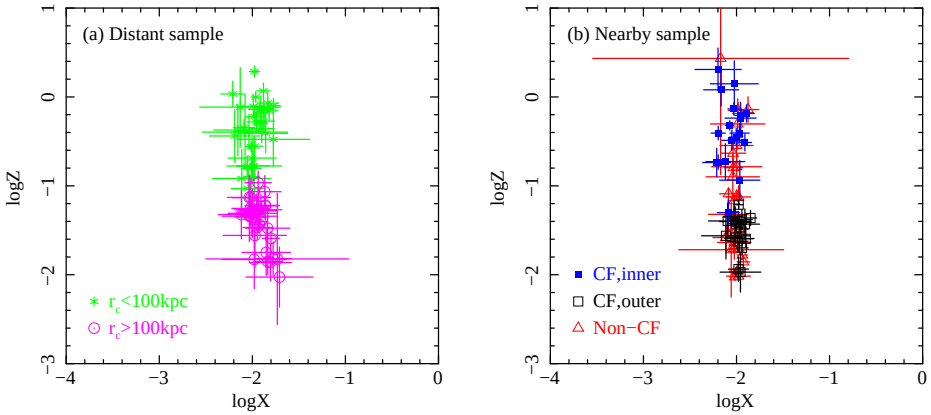

Fig. 6 X-ray fundamental plane for the distant cluster sample (Ota et al. 2006) and the nearby sample compiled by Mohr et al. (1999). The distribution of the clusters projected onto the $\log X - \log Z$ plane is shown in each panel. For the nearby sample, according to table 2 of Mohr et al. (1999), non cooling-flow clusters are shown with the red triangles, and inner-core and outer-core components of cooling-flow clusters are separately shown with the solid blue boxes and open black boxes.

(1999), implying that the clusters form a two-parameter family. Applying this technique to distant clusters at $z > 0.1$, Ota et al. (2006) obtained the following three orthogonal parameters:

$$X \propto n_{e0}^{0.44}\, r_{\rm c}^{0.65}\, T^{-0.62}\,, \tag{35}$$

$$Y \propto n_{e0}^{0.45}\, r_{\rm c}^{0.44}\, T^{0.78}\,, \tag{36}$$

$$Z \propto n_{e0}^{0.78}\, r_{\rm c}^{-0.62}\, T^{-0.10} \tag{37}$$

and also confirmed the presence of the X-ray fundamental plane for the distant cluster sample. The distribution of clusters projected onto the $X - Z$ plane is shown in Figure 6. The Z-axis of the plane is called the principal axis and represents the direction along which the dispersion of the data points becomes the largest in the 3D space. By setting $X \sim$ constant, Equation (37) yields $Z \propto r_{\rm c}^{-1.78}\, T^{-0.10} \propto n_{e0}^{1.20}\, T^{-0.69}$. Since the radiative cooling time is $t_{\rm cool} \propto T^{1/2} n_{e0}^{-1}$, it is rewritten as

$$Z \propto t_{\rm cool}^{-1.2}\,. \tag{38}$$

Therefore $t_{\rm cool}$ is considered to be a key parameter to control the cluster's gas evolution. A trend of morphological change of X-ray clusters along the $t_{\rm cool}$-axis is actually observed (Ota et al. 2006). Hudson et al. (2010) noted that the cooling time is the most suitable parameter to segregate CC/NCC clusters, which is in agreement with the above result.

It should be noted that a cool core is also found in some irregular clusters. This phenomenon is interpreted as a remnant of a merging core and may be used to diagnose the merging history (e.g., Markevitch & Vikhlinin 2007).

3.3 Beyond the β-model: Observed Gas Profiles and the Possibility of Quasi-hydrostatic Cooling

To better reproduce observed X-ray surface brightness profiles, some authors have introduced empirical models such as the double-β model (Jones & Forman 1984) and the modified β model (Vikhlinin

et al. 2006). For the latter, they modified the original β-profile by adding a cool density cusp at the center and steepening the slope at a large radius. This model gave a good fit to spatially-resolved spectroscopic and imaging data taken with *Chandra* for its large radial range including the core emission (see also Bulbul et al. 2010).

Given that radiative cooling plays an important role in the thermodynamical evolution of ICM, how are the cool cores actually formed and maintained? The possibility of quasi-hydrostatic cooling in the cluster core was first noted by Masai & Kitayama (2004). Unlike isobaric cooling flows that increase the local density so the thermal pressure $P(r)$ counteracts the local cooling, quasi-hydrostatic cooling allows the gas to modify its profile or core size so $\nabla P(r)$ balances the gravitational force. The inflow is so moderate that the hydrostatic balance is not disturbed significantly. The quasi-hydrostatic model predicts a temperature profile that approaches a constant temperature of $\sim 1/3$ that of ambient, non-cooling gas, which agrees with those derived from X-ray observations of relaxed clusters (Kaastra et al. 2004; Allen et al. 2001; Tamura et al. 2001). Using a hydrodynamics code, Akahori & Masai (2006) investigated the evolution of the core structure of radiatively cooling gas. They suggested a radiative-cooling origin for the appearance of a small ($r_c \sim 50$ kpc) core, while cooling is not important in clusters with large cores. Their simulations also showed that the cluster core maintains the quasi-hydrostatic condition before the initial central cooling time has elapsed. This result gives a possible interpretation of the observed double-peaked distribution of core size.

Arnaud et al. (2010) discussed the universal pressure profile for the REXCESS cluster sample, and obtained the best-fit profile based on the generalized NFW model by Nagai et al. (2007). For the scaled temperature and the density, Arnaud et al. (2010) found that their deviations from the average scaled profile are anti-correlated with each other in the core, $r/r_{500} < 0.2$ (fig. 3 in their paper); the anti-correlation is more clearly seen for cool core clusters. This behavior is supported by the quasi-hydrostatic cooling picture.

Since the cooling time is shorter than the Hubble time for the CC clusters, some heating is needed to sustain the system, otherwise it would disappear $\sim$Gyr after becoming virialized. Practically, however, heating due to mergers is likely invoked in the cluster's evolution. The clusters of core radii > 400 kpc in the histogram (Fig. 5) are attributed to mergers from their irregular morphology. Recently, the process of cyclic evolution between CC and NCC clusters was proposed by Rossetti et al. (2011) taking account of the lifetime of diffuse radio emission.

3.4 Entropy Profiles

Measurement of a gas entropy profile provides important information on the evolution of gas since it determines the structure of intracluster gas and records the thermal history. The gas entropy, S, in the field of cluster research is defined by

$$S = kTn_{\rm e}^{-2/3}\,, \tag{39}$$

and is different from the original definition in the field of thermodynamics.

The gravitational heating, namely conversion of the potential energy to thermal energy, should depend on the depth of the gravitational potential, which is approximated by the virial temperature of the system. The entropy generation due to gravitational collapse is predicted to be self-similar and follows a power-law form $S(r) \propto r^{1.1}$ (Tozzi & Norman 2001; Voit 2005). Thus deviations from this *baseline* distribution may be attributed to cooling and heating processes in the cluster. Earlier results on groups and clusters observed with ROSAT showed that smaller systems like groups have entropy excess called the "entropy floor" at the center while the slope of the distribution follows the $\propto r^{1.1}$ law (Ponman et al. 2003). Thus the non-gravitational effects, preheating or galaxy feedbacks, are considered to play a greater role in smaller systems.

More systematic studies of entropy profiles with a large number of clusters have been carried out; Cavagnolo et al. (2009) derived radial entropy profiles of ICM for 239 clusters with the

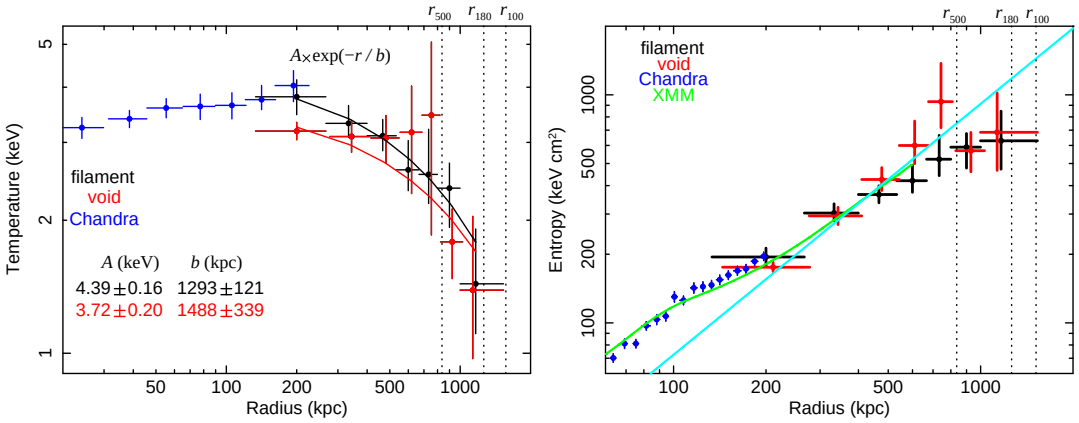

Fig. 7 Radial temperature and entropy profiles of the Hydra A cluster measured with *Suzaku* (Sato et al. 2012). The results for filament (*black*) and void (*red*) directions are shown. The *Chandra* results (David et al. 2001) are plotted in blue.

Chandra data (the ACCEPT sample) and found that that most entropy profiles are well fitted by a model consisting of a power-law plus a constant, $K(r) = K_0 + K_{100}(r/100\ \mathrm{kpc})^{\alpha}$. The best-fit parameters are $(K_0, K_{100}, \alpha) = (16.1, 150, 1.20), (156, 107, 1.23)$ for clusters with $K_0 \leq 50$ and $K_0 > 50\ \mathrm{keV\,cm^2}$, respectively. They also showed that the distribution of central entropy K_0 is bimodal, which peaks at $K_0 \sim 15\ \mathrm{keV\,cm^2}$ and $\sim 150\ \mathrm{keV\,cm^2}$. A similar two peaked distribution has been found in the REXCESS sample observed with *XMM-Newton* (Pratt et al. 2010). Pratt et al. (2006) measured the entropy profile in relaxed clusters to find that outside $0.1r_{200}$ the scaled entropy profile is consistent with gravitational heating while the scatter increases with smaller radius and suggested that the results agree with models of accretion shock.

The advent of the *Suzaku* satellite (Mitsuda et al. 2007) enables the measurement of gas properties out to large radii because of its low background level and high sensitivity. The temperature and entropy distributions up to the virial radius have been derived for massive clusters (George et al. 2009; Reiprich et al. 2009; Bautz et al. 2009; Kawaharada et al. 2010b; Hoshino et al. 2010; Simionescu et al. 2011; Akamatsu et al. 2011). The latest result from Hydra A (Sato et al. 2012) is shown in Figure 7. For those clusters observed with *Suzaku*, a systematic drop in temperature by a factor of about three from outside the core to r_{200} was found and the entropy profiles become flatter beyond r_{500} in comparison with the $r^{1.1}$ profile. Some explanations for observed low entropy are proposed and discussed: in-falling matter retains some of its kinetic energy in the form of bulk motion (Kawaharada et al. 2010b), a gas clumping effect (Simionescu et al. 2011), and deviation of electron temperature from ion temperature (Akahori & Yoshikawa 2010).

4 CLUSTER MERGER AND SEARCH FOR NON-THERMAL PHENOMENA

According to the standard scenario of cosmic structure formation, clusters are believed to have grown into their present shape via collisions and mergers of smaller groups and clusters. A cluster merger has a kinetic energy of the order of

$$E \sim \frac{1}{2}(M_1 + M_2)v^2 \sim 10^{65}\ \mathrm{erg} \left(\frac{M_1 + M_2}{10^{15}\ M_\odot}\right) \left(\frac{v}{3000\ \mathrm{km\ s^{-1}}}\right)^2 , \qquad (40)$$

where M_1 and M_2 are masses of two objects. v is the collision speed and $v = 3000\ \mathrm{km\ s^{-1}}$ corresponds to a mach number of 2–3 in the intracluster medium. This is the most energetic event in the

Universe since the Big Bang. If two such objects collide with each other under their mutual gravitational attraction, a huge amount of energy may be released and a certain fraction is expected to heat the gas and generate non-thermal particles through shock waves, and induce bulk and turbulent gas motions.

We can recognize signatures of merging in many ways. In X-rays, irregular morphology and the complex temperature structure of gas tell us that the system is disturbed due to the past mergers. The most prominent shock feature has been detected in 1E0657–56 (the Bullet Cluster; Markevitch et al. 2002). The bow shock propagates in front of a bullet-like gas and significant jumps in temperature and density have been found. The displacement between the peak positions of X-ray gas and dark matter distributions have been identified in merging systems such as the Bullet cluster and A2744 (Merten et al. 2011), which provide an opportunity to constrain the self-interaction cross section of dark matter particles.

4.1 Gas Bulk Motion and Turbulence

In the course of merging, different portions of the hot gas are predicted to collide with each other at a relative speed of $\sim$ a few $\times 1000\ \mathrm{km\ s^{-1}}$, which will persist for several Gyrs after each merger event (Norman & Bryan 1999). If the gas has a large bulk velocity compared to its sound velocity, non-thermal pressure can no longer be neglected and has to be taken into account in estimating the cluster's mass. Suppose, for simplicity, that the gas is rigidly rotating with a circular velocity of $\sigma_r (\propto r)$, then the balance against the gravitational pull at radius r on the rotational equatorial plane then becomes

$$-\frac{GM(r)}{r^2} = \frac{1}{\rho_{\rm gas}}\frac{\partial}{\partial r} P_{\rm gas}(1 + f\beta_r)\,, \tag{41}$$

where

$$\beta_r \equiv \frac{\mu m_p \sigma_r^2}{kT} \sim 1.07 \left(\frac{\mu}{0.63}\right)\left(\frac{\sigma_r}{700\ \mathrm{km\ s^{-1}}}\right)\left(\frac{kT}{3\ \mathrm{keV}}\right)^{-1} \tag{42}$$

and f is the fraction of gas that is rotating (Ota et al. 2007). Therefore the hydrostatic mass needs to be modified by a factor of $(1 + f\beta_r)$ given the presence of kinetic gas motion.

It is essential to constrain the gas motion through observations. The cluster gas contains a large amount of heavy elements such as iron, silicon, and oxygen etc. If the gas has a velocity along the line of sight, it produces Doppler shifts in emission lines from the heavy ions. The line shift due to the line-of-sight bulk velocity $v_{\rm turb}$ can be expressed as follows

$$\Delta E_{\rm bulk} = E_0 \frac{v_{\rm bulk}}{c} = 6.7\ \mathrm{eV} \left(\frac{E_0}{6.7\ \mathrm{keV}}\right)\left(\frac{v_{\rm bulk}}{300\ \mathrm{km\ s^{-1}}}\right)\,, \tag{43}$$

where E_0 denotes the rest-frame energy of the line emission. For example, a line shift due to the bulk velocity of $1000\ \mathrm{km\ s^{-1}}$ corresponds to a shift in the 6.7 keV Fe-K line energy of 22 eV. On the other hand, line broadenings due to turbulent and thermal motions are given by the following two equations:

$$\Delta E_{\rm turb} = E_0 \frac{v_{\rm bulk}}{c} = 6.7\ \mathrm{eV} \left(\frac{E_0}{6.7\ \mathrm{keV}}\right)\left(\frac{v_{\rm turb}}{300\ \mathrm{km\ s^{-1}}}\right)\,, \tag{44}$$

$$\Delta E_{\rm th} = E_0 \frac{\sqrt{kT/m}}{c} = 3\ \mathrm{eV} \left(\frac{E_0}{6.7\ \mathrm{keV}}\right)\left(\frac{kT}{5\ \mathrm{keV}}\right)^{1/2}\left(\frac{m}{56 m_p}\right)^{-1}\,. \tag{45}$$

Because the thermal width is inversely related to the ion mass m, the ratio of turbulent broadening to the thermal broadening, $\Delta E_{\rm turn}/\Delta E_{\rm th}$, becomes larger for larger m. Thus the Fe emission line is the best-suited line for velocity diagnostics in clusters.

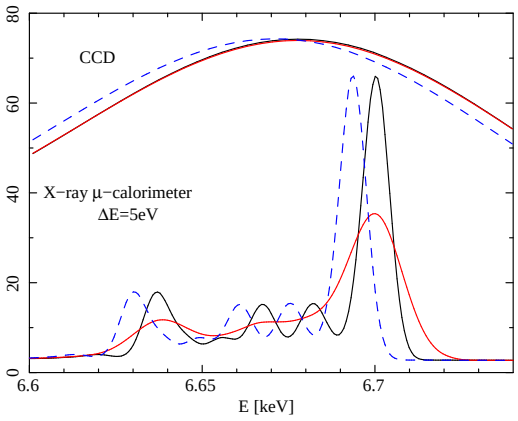

Fig. 8 6.7 keV Fe XXV line profiles for $kT = 5$ keV thermal gas convolved with the typical CCD and calorimeter detector responses. (i) thermal broadening only (*black*), (ii) thermal broadening + bulk motion $v_{\rm bulk} = 300\ {\rm km\ s^{-1}}$ (*blue*), (iii) thermal broadening + turbulent broadening $v_{\rm turb} = 300\ {\rm km\ s^{-1}}$ (*red; color online*).

Figure 8 shows the Fe emission line model convolved with instrumental responses assuming an X-ray CCD resolution of 130 eV and an X-ray micro-calorimeter resolution of 5 eV (FWHM).

By measuring the energy shift with X-ray spectroscopy, one can directly probe the dynamical state of the gas. However, it is not easy since it requires not only a high energy resolution and a good sensitivity but also a precise instrumental energy-gain calibration. Based on the careful assessment of positional gain variation of the *Suzaku* XIS detector (Koyama et al. 2007), a tight constraint on the bulk velocity with an accuracy of $700\ {\rm km\ s^{-1}}$ has been placed in the central region of the Centaurus cluster (Ota et al. 2007). They placed the upper limit on the line-of-sight velocity difference at $1400\ {\rm km\ s^{-1}}$. Hence, cluster mass estimation under a hydrostatic assumption is justified within a factor of about two–three. The Doppler-shift measurement using the Fe line has been carried out in several nearby clusters: Sato et al. (2008); Sugawara et al. (2009); Sato et al. (2011) derived the upper limit on the bulk velocity, and Dupke et al. (2007); Dupke & Bregman (2006) reported possible detection of bulk gas flow. Recently, the significant bulk velocity of a subcluster region relative to the main cluster, $\sim 1500\ {\rm km\ s^{-1}}$, has been detected in A2256 by *Suzaku* (Tamura et al. 2011).

The turbulent motion has been probed by measuring a spatially-resolved gas pressure map in the Coma cluster (Schuecker et al. 2004). The pressure fluctuation spectrum is found to be consistent with the Kolmogorov spectrum, yielding the lower limit of 10% of the total gas pressure in turbulent form. The turbulent line broadening has been constrained using the Reflection Grating Spectrometer (RGS) on *XMM-Newton* in the central regions of ellipticals, groups and clusters (Sanders et al. 2011). They placed a strong upper limit on the turbulent motion ($< 200\ {\rm km\ s^{-1}}$) for several objects while line broadening has been found in Klemola 44 and a weak signature in RX J1347–1145.

Theoretical expectation for line shifting and broadening associated with turbulence and bulk motions as well as their detectability are discussed by Sunyaev et al. (2003); Inogamov & Sunyaev (2003); Dolag et al. (2005); Pawl et al. (2005).

4.2 Non-thermal Hard X-ray Emission

At radio wavelengths, synchrotron emissions extending over a Mpc scale have been discovered from more than 30 clusters (Giovannini et al. 1999). The existence of radio halo emission suggests that

relativistic electrons are being accelerated in the intracluster space. Interestingly, there is a correlation between the radio synchrotron power (non-thermal, $P_{1.4}$) and X-ray luminosity (thermal, $L_{\rm X}$) for merging clusters while relaxed clusters without a radio halo lie in a region well separated from the merging clusters on the $P_{1.4} - L_{\rm X}$ plane (Brunetti et al. 2009). It is suggested that the generation of high-energy particles is connected to the dynamical evolution of clusters (Cassano et al. 2010).

In X-rays, the same population of high-energy electrons is thought to interact with 3K CMB photons and then generate non-thermal Inverse-Compton (IC) emission. The IC emission in excess of the thermal emission is then predicted to be seen in the hard X-ray band ($>\sim 10$ keV) where the thermal emission normally diminishes because of the exponential cutoff in the continuum spectrum (Eq. (8)). In addition, from the radio observation alone, we cannot separate the energy of magnetic fields from the energy of high-energy electrons. However, by comparing the radio and hard X-ray fluxes ($S_{\rm syn}$ and $S_{\rm IC}$), the cluster's magnetic field can be estimated using the assumption that the same population of relativistic electrons scatter off of CMB photons since the ratio $S_{\rm syn}/S_{\rm IC}$ is equal to the ratio between the energy density of the magnetic field and the CMB

$$S_{\rm syn}/S_{\rm IC} = U_B/U_{\rm CMB} \tag{46}$$

(Rybicki & Lightman 1985). $U_B = (B^2/8\pi)$ and $U_{\rm CMB} = 4.2\times10^{-13}(1+z)^4\,{\rm erg\,cm^{-3}}$. The exact derivations of the synchrotron and IC emissions at a certain frequency are presented in Blumenthal & Gould (1970).

The existence of non-thermal IC hard X-rays in the Coma cluster has been pointed out from *RXTE* (Rephaeli & Gruber 2002) and *BeppoSAX* observations (Fusco-Femiano et al. 2004). Recent reports based on the broadband X-ray observations with *Suzaku* (Wik et al. 2009) and Swift (Wik et al. 2011) did not find any significant non-thermal hard X-ray emission and the hard X-ray flux is reproduced by thermal models. It is suggested that this discrepancy between satellites can be reconciled if different sizes of field-of-views are taken into consideration (Fusco-Femiano et al. 2011).

Non-thermal hard X-ray emission has been constrained in about 10 bright clusters with *Suzaku*. The Hard X-ray Detector (HXD) on *Suzaku* has a field of view of $34' \times 34'$ (FWHM) at energies below 100 keV and has achieved the lowest background level (Takahashi et al. 2007).

Figure 9 shows the hard X-ray spectrum of the hottest Abell cluster A2163 ($z = 0.203$) obtained with the *Suzaku* HXD. The additional power-law component does not significantly improve the fit and the observed hard X-ray spectrum is well explained by the multi-temperature thermal model, giving the upper limit on the IC emission. This is consistent with the previous report by *BeppoSAX* (Feretti et al. 2001). The HXD results (Kitaguchi et al. 2007; Fujita et al. 2008; Kawano et al. 2009; Nakazawa et al. 2009; Sugawara et al. 2009; Wik et al. 2009; Kawaharada et al. 2010a) are compared with those from other satellites, *RXTE*, *BeppoSAX*, and Swift in Figure 10. There is no firm detection of the IC emission reported for these 10 objects from *Suzaku*. The cluster magnetic field obtained through the synchrotron-IC measurement (Eq. (46)) based on the *Suzaku* HXD observations is also plotted in the figure. Note that the estimation of magnetic field may be affected by the assumption of index p of the electron distribution, $N(\gamma) = N_0\gamma^{-p}$ (γ is the Lorentz factor of the electron).

The situation of non-thermal X-rays from clusters remains uncertain, and higher sensitivity in the high-energy range is required to further explore the physics of gas heating and particle acceleration in clusters.

4.3 Super-hot Thermal Gas in Violent Mergers

The study of thermal structure in clusters offers important perspectives on understanding the merging configuration and heating process of the cluster's gas. Merger shock and evolution of temperature structure for ions and electrons have been studied by numerical simulations. Given high sound velocity in the intracluster medium, it does not seem easy for an in-falling sub cluster to

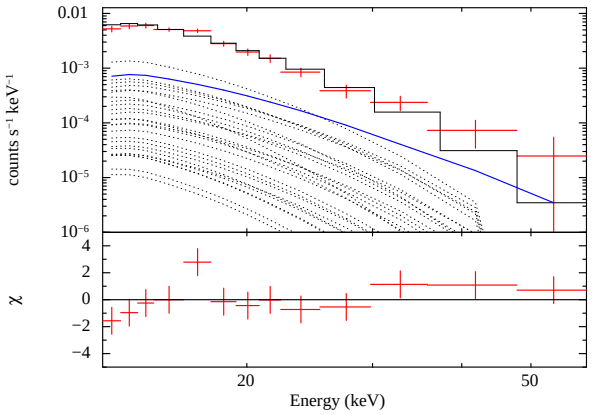

Fig. 9 *Suzaku* HXD spectrum of the hot cluster of galaxies A2163. Significant emission is detected up to about $\sim$ 50 keV. The spectral model consisting of multi-temperature thermal plasma (*many thin dotted black lines*) plus a non-thermal power-law component (*blue; color online*) is indicated.

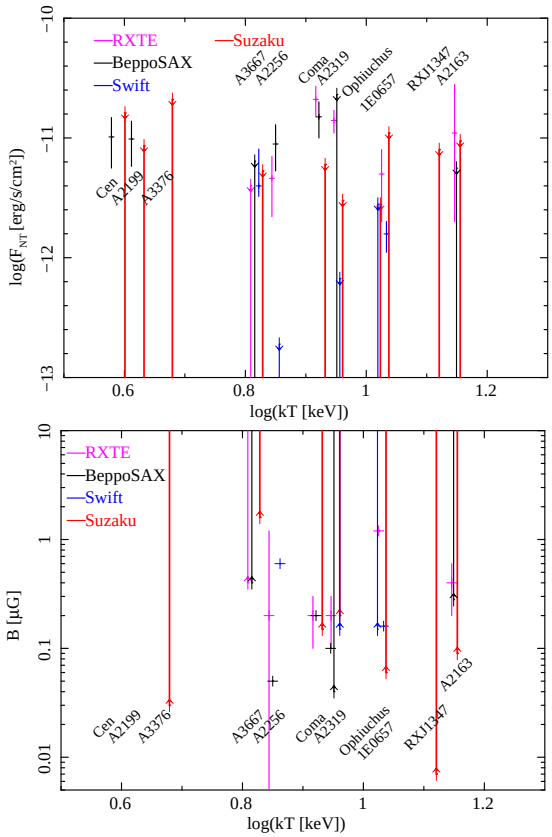

Fig. 10 Non-thermal IC hard X-ray flux and cluster magnetic field in 10 clusters obtained with *Suzaku* (*red*). For *Suzaku*, the results are quoted from Kitaguchi et al. (2007); Fujita et al. (2008); Ota et al. (2008); Kawano et al. (2009); Nakazawa et al. (2009); Sugawara et al. (2009); Wik et al. (2009); Kawaharada et al. (2010a), Ota et al. in prep., and Nagayoshi et al. in prep. For Swift (*blue*), Ajello et al. (2009, 2010); Wik et al. (2011). For *RXTE* (*magenta*) and *BeppoSAX* (*black*), see Rephaeli et al. (2008); references therein.

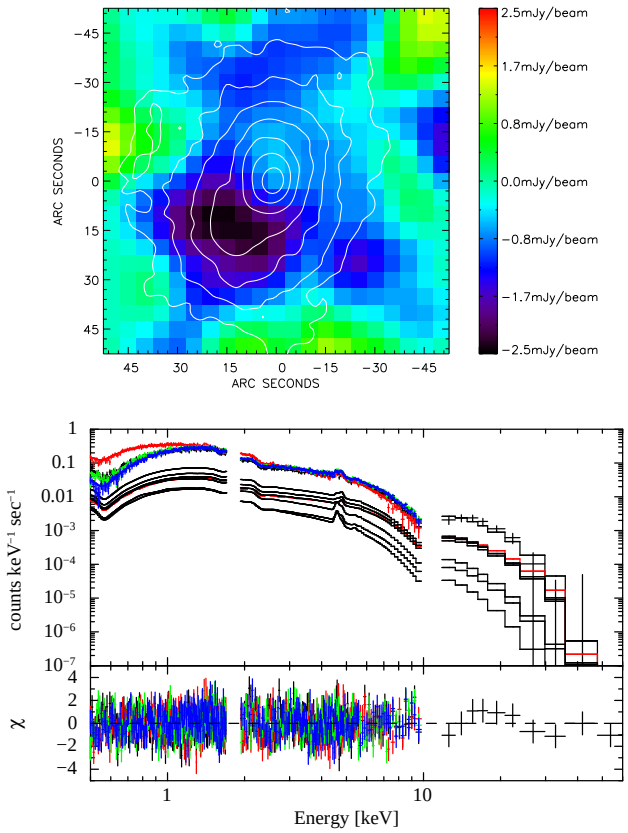

Fig. 11 High-resolution SZ effect map taken at the 45-m Nobeyama telescope (*top; Kitayama et al. 2004)* and *Suzaku* broadband spectra of the most X-ray luminous cluster RX J1347–1145 (*bottom; Ota et al. 2008)*. The XIS data below 10 keV and the HXD data above 10 keV are shown with crosses. The step functions show the best-fit thermal model consisting of multi-temperature components for the ambient gas (*many black lines*) plus the very hot thermal gas (*red line*) identified in the South-East region of the cluster (see also Fig. 1 right).

acquire a high enough Mach number to form strong shocks. On the other hand, there are some pieces of observational evidence for strongly heated gas that is likely to be generated by high-speed ($> 2000\,\mathrm{km\,s^{-1}}$) collisions.

The presence of extremely hot gas in the most X-ray luminous cluster RX J1347–1145 has been confirmed by the *Suzaku* broadband spectroscopy (Fig. 11; Ota et al. 2008). From the joint analysis of the *Suzaku* and *Chandra* data, the temperature of a hot clump (Fig. 1 right) is measured to be about 25 keV, which is more than two times higher than the temperature of the surrounding gas. This unexpectedly high-temperature gas has been pointed out previously by observations of the Sunyaev-Zel'dovich (SZ) effect (Komatsu et al. 2001; Kitayama et al. 2004), and the broadband X-ray data have improved the accuracy by 3-fold. Importantly, the X-ray spectrum of this hot component is more accurately represented by a thermal emission model rather than a non-thermal power-law model. The results support a scenario that this cluster has experienced a recent violent merger as the very hot gas is over-pressured and predicted to be short-lived (~ 0.5 Gyr) (Takizawa 1999). It is also worth noting that super-hot thermal gas significantly contributes to the hard X-ray flux, which needs to be precisely modeled in the search for non-thermal IC emission. Under the detailed multi-temperature

modeling of thermal emission components, non-thermal IC emission is not found to be significant in the hard X-ray spectra obtained with *Suzaku* for RX J1347–1145 (Ota et al. 2008), Coma (Wik et al. 2009), Abell 2163 (Ota et al. in prep.) and the Bullet cluster (Nagayoshi et al. in prep.).

Is very hot gas commonly seen in merging systems? In a nearby merging cluster A3667, a similar hot (> 13 keV) thermal component is suggested from the *Suzaku* observations (Nakazawa et al. 2009). Including a shock-front cluster, the Bullet cluster, the *Chandra* and *XMM-Newton* temperature maps show that some clusters contain very hot (> 10 keV) gas. The *Chandra* analysis by Million & Allen (2009) indicated that the hard excess can be attributed to non-thermal gas or quasi-thermal gas with $kT > 20$ keV.

The collision velocity necessary to explain such super-hot thermal gas due to strong shock heating is high ($\sim 3000 - 4000\,\mathrm{km\ s^{-1}}$), which challenges the Lambda CDM model of cosmology (Lee & Komatsu 2010).

5 FUTURE PROSPECTS

X-ray spectroscopy and imaging observations bring us rich information on the nature of galaxy clusters, not only about the baryonic content but also concerning dark matter that governs the mass structure of the objects. Large-scale cluster surveys in various wavelengths are now on-going or planned, aiming to reveal the structural evolution of the Universe and obtaining more stringent limits on cosmological parameters. The baryonic mass fraction and cluster abundance as a function of redshift have been used to constrain the dark matter and dark energy densities as well as the dark energy equation of state. These measurements require precise mass estimates of large numbers of clusters, and thus understanding the physical state of intracluster gas to calibrate scatter and redshift evolution and uncover any bias in relationships between cluster mass and observables (e.g., Majumdar & Mohr 2003).

Overall, clusters are *regular* objects, having positive correlations between global quantities (gas temperature, bolometric luminosity, gas mass etc.) and the total mass derived either from X-ray observations or a gravitational lensing effect. However, deviations from the self-similar expectations have been observed in terms of the power-law slopes and scatters around them. They are considered to have originated from non-gravitational effects like radiative cooling, feedback from galaxies, bulk and turbulent gas motions, magnetic field support etc.

Among these issues, measurement of velocity structure to high accuracy is expected to be carried out by future high-resolution spectroscopy using an X-ray micro-calorimeter. The ASTRO-H satellite is scheduled to be launched in 2014 (Takahashi et al. 2010) and will play a critical role in revealing the dynamics of clusters. The Soft X-ray Spectrometer (SXS) onboard ASTRO-H is a non-dispersive spectrometer and enables high-resolution (5 eV) observations for both point sources and diffuse objects (Mitsuda et al. 2010). SXS will measure the kinetic gas motions to an accuracy of $\sim 100\ \mathrm{km\ s^{-1}}$ through observations of line emissions. The Hard X-ray Imager on ASTRO-H (Kokubun et al. 2010) will constrain the non-thermal high-energy contents in clusters with its imaging spectroscopy in the hard X-ray band. Now NuStar (Harrison et al. 2010) is successfully in orbit and draws peoples' attention to upcoming observations with the first focusing telescope in the high energy X-ray regime. The eROSITA on the Spectrum-Roentgen-Gamma mission will perform an all-sky survey in the X-ray energy range and detect $\sim 100\,000$ clusters (Predehl et al. 2010). In conjunction with optical and SZ surveys, the next-generation X-ray missions will largely enhance the study of clusters and lead us to draw a more complete view of structure formation and evolution in the Universe.

Acknowledgements N.O. acknowledges the editors for giving me opportunity to write this review article.

References

Ajello, M., Rebusco, P., Cappelluti, N., et al. 2009, ApJ, 690, 367
Ajello, M., Rebusco, P., Cappelluti, N., et al. 2010, ApJ, 725, 1688
Akahori, T., & Masai, K. 2005, PASJ, 57, 419
Akahori, T., & Masai, K. 2006, PASJ, 58, 521
Akahori, T., & Yoshikawa, K. 2010, PASJ, 62, 335
Akamatsu, H., Hoshino, A., Ishisaki, Y., et al. 2011, PASJ, 63, 1019
Allen, S. W., Schmidt, R. W., & Fabian, A. C. 2001, MNRAS, 328, L37
Anders, E., & Grevesse, N. 1989, Geochim. Cosmochim. Acta, 53, 197
Arnaud, M., Pointecouteau, E., & Pratt, G. W. 2005, A&A, 441, 893
Arnaud, M., Pratt, G. W., Piffaretti, R., et al. 2010, A&A, 517, A92
Bautz, M. W., Miller, E. D., Sanders, J. S., et al. 2009, PASJ, 61, 1117
Blumenthal, G. R., & Gould, R. J. 1970, Reviews of Modern Physics, 42, 237
Böhringer, H., & Werner, N. 2010, A&A Rev., 18, 127
Brunetti, G., Cassano, R., Dolag, K., & Setti, G. 2009, A&A, 507, 661
Bulbul, G. E., Hasler, N., Bonamente, M., & Joy, M. 2010, ApJ, 720, 1038
Cassano, R., Ettori, S., Giacintucci, S., et al. 2010, ApJ, 721, L82
Cavagnolo, K. W., Donahue, M., Voit, G. M., & Sun, M. 2009, ApJS, 182, 12
Cavaliere, A., & Fusco-Femiano, R. 1976, A&A, 49, 137
Chen, Y., Reiprich, T. H., Böhringer, H., Ikebe, Y., & Zhang, Y.-Y. 2007, A&A, 466, 805
David, L. P., Nulsen, P. E. J., McNamara, B. R., et al. 2001, ApJ, 557, 546
Dolag, K., Vazza, F., Brunetti, G., & Tormen, G. 2005, MNRAS, 364, 753
Dupke, R. A., & Bregman, J. N. 2006, ApJ, 639, 781
Dupke, R. A., Mirabal, N., Bregman, J. N., & Evrard, A. E. 2007, ApJ, 668, 781
Evrard, A. E., Metzler, C. A., & Navarro, J. F. 1996, ApJ, 469, 494
Fabian, A. C. 1994, ARA&A, 32, 277
Feretti, L., Fusco-Femiano, R., Giovannini, G., & Govoni, F. 2001, A&A, 373, 106
Fujita, Y., Hayashida, K., Nagai, M., et al. 2008, PASJ, 60, 1133
Fujita, Y., & Takahara, F. 1999, ApJ, 519, L51
Fusco-Femiano, R., Orlandini, M., Brunetti, G., et al. 2004, ApJ, 602, L73
Fusco-Femiano, R., Orlandini, M., Bonamente, M., & Lapi, A. 2011, ApJ, 732, 85
George, M. R., Fabian, A. C., Sanders, J. S., Young, A. J., & Russell, H. R. 2009, MNRAS, 395, 657
Giovannini, G., Tordi, M., & Feretti, L. 1999, New Astron., 4, 141
Gunn, J. E., & Gott, J. R., III 1972, ApJ, 176, 1
Harrison, F. A., Boggs, S., Christensen, F., et al. 2010, in Society of Photo-Optical Instrumentation Engineers (SPIE) Conference Series, Space Telescopes and Instrumentation 2010: Ultraviolet to Gamma Ray, eds. M. Arnaud, S. S. Murray, & T. Takahashi, 7732, 77320S
Hattori, M., Kneib, J., & Makino, N. 1999, Progress of Theoretical Physics Supplement, 133, 1
Hoshino, A., Henry, J. P., Sato, K., et al. 2010, PASJ, 62, 371
Hudson, D. S., Mittal, R., Reiprich, T. H., et al. 2010, A&A, 513, A37
Ikebe, Y., Makishima, K., Fukazawa, Y., et al. 1999, ApJ, 525, 58
Inogamov, N. A., & Sunyaev, R. A. 2003, Astronomy Letters, 29, 791
Jee, M. J., Ford, H. C., Illingworth, G. D., et al. 2007, ApJ, 661, 728
Jones, C., & Forman, W. 1984, ApJ, 276, 38
Kaastra, J. S. 1992, An X-Ray Spectral Code for Optically Thin Plasmas (Internal SRON-Leiden Report, updated version 2.0), 2
Kaastra, J. S., Mewe, R., & Nieuwenhuijzen, H. 1996, in UV and X-ray Spectroscopy of Astrophysical and

Laboratory Plasmas, eds. K. Yamashita, & T. Watanabe, 411
Kaastra, J. S., Tamura, T., Peterson, J. R., et al. 2004, A&A, 413, 415
Kawaharada, M., Makishima, K., Kitaguchi, T., et al. 2010a, PASJ, 62, 115
Kawaharada, M., Okabe, N., Umetsu, K., et al. 2010b, ApJ, 714, 423
Kawano, N., Fukazawa, Y., Nishino, S., et al. 2009, PASJ, 61, 377
King, I. 1962, AJ, 67, 471
Kitaguchi, T., Nakazawa, N., Makishima, K., et al. 2007, in XMM-Newton: The Next Decade, 28P
Kitayama, T., Komatsu, E., Ota, N., et al. 2004, PASJ, 56, 17
Kneib, J.-P., & Natarajan, P. 2011, A&A Rev., 19, 47
Kokubun, M., Nakazawa, K., Enoto, T., et al. 2010, in Society of Photo-Optical Instrumentation Engineers (SPIE) Conference Series, Space Telescopes and Instrumentation 2010: Ultraviolet to Gamma Ray, eds. M. Arnaud, S. S. Murray, & T. Takahashi, 7732, 773215
Komatsu, E., Matsuo, H., Kitayama, T., et al. 2001, PASJ, 53, 57
Komatsu, E., Smith, K. M., Dunkley, J., et al. 2011, ApJS, 192, 18
Koyama, K., Tsunemi, H., Dotani, T., et al. 2007, PASJ, 59, 23
Larson, D., Dunkley, J., Hinshaw, G., et al. 2011, ApJS, 192, 16
Lee, J., & Komatsu, E. 2010, ApJ, 718, 60
Liedahl, D. A., Osterheld, A. L., & Goldstein, W. H. 1995, ApJ, 438, L115
Lodders, K. 2003, ApJ, 591, 1220
Majumdar, S., & Mohr, J. J. 2003, ApJ, 585, 603
Makino, N., Sasaki, S., & Suto, Y. 1998, ApJ, 497, 555
Markevitch, M., & Vikhlinin, A. 2007, Phys. Rep., 443, 1
Markevitch, M., Gonzalez, A. H., David, L., et al. 2002, ApJ, 567, L27
Masai, K., & Kitayama, T. 2004, A&A, 421, 815
McNamara, B. R., Wise, M., Nulsen, P. E. J., et al. 2000, ApJ, 534, L135
Merten, J., Coe, D., Dupke, R., et al. 2011, MNRAS, 417, 333
Mewe, R., Gronenschild, E. H. B. M., & van den Oord, G. H. J. 1985, A&AS, 62, 197
Mewe, R., Lemen, J. R., & van den Oord, G. H. J. 1986, A&AS, 65, 511
Million, E. T., & Allen, S. W. 2009, MNRAS, 399, 1307
Mitsuda, K., Bautz, M., Inoue, H., et al. 2007, PASJ, 59, 1
Mitsuda, K., Kelley, R. L., Boyce, K. R., et al. 2010, in Society of Photo-Optical Instrumentation Engineers (SPIE) Conference Series, Space Telescopes and Instrumentation 2010: Ultraviolet to Gamma Ray, eds. M. Arnaud, S. S. Murray, & T. Takahashi, 7732, 773211
Mohr, J. J., Mathiesen, B., & Evrard, A. E. 1999, ApJ, 517, 627
Moore, B., Calcáneo-Roldán, C., Stadel, J., et al. 2001, Phys. Rev. D, 64, 063508
Mushotzky, R. F., & Loewenstein, M. 1997, ApJ, 481, L63
Nagai, D., Kravtsov, A. V., & Vikhlinin, A. 2007, ApJ, 668, 1
Nakamura, T. T., & Suto, Y. 1997, Progress of Theoretical Physics, 97, 49
Nakazawa, K., Sarazin, C. L., Kawaharada, M., et al. 2009, PASJ, 61, 339
Navarro, J. F., Frenk, C. S., & White, S. D. M. 1997, ApJ, 490, 493
Neumann, D. M., & Arnaud, M. 1999, A&A, 348, 711
Norman, M. L., & Bryan, G. L. 1999, in The Radio Galaxy Messier 87, Lecture Notes in Physics, 530, eds. H.-J. Röser, & K. Meisenheimer (Berlin: Springer Verlag) 106
O'Hara, T. B., Mohr, J. J., Bialek, J. J., & Evrard, A. E. 2006, ApJ, 639, 64
Ota, N., Pointecouteau, E., Hattori, M., & Mitsuda, K. 2004, ApJ, 601, 120
Ota, N., Kitayama, T., Masai, K., & Mitsuda, K. 2006, ApJ, 640, 673
Ota, N., Fukazawa, Y., Fabian, A. C., et al. 2007, PASJ, 59, 351
Ota, N., Murase, K., Kitayama, T., et al. 2008, A&A, 491, 363

Ota, N., & Mitsuda, K. 2002, ApJ, 567, L23
Ota, N., & Mitsuda, K. 2004, A&A, 428, 757
Pawl, A., Evrard, A. E., & Dupke, R. A. 2005, ApJ, 631, 773
Peterson, J. R., & Fabian, A. C. 2006, Phys. Rep., 427, 1
Ponman, T. J., Sanderson, A. J. R., & Finoguenov, A. 2003, MNRAS, 343, 331
Pratt, G. W., Arnaud, M., & Pointecouteau, E. 2006, A&A, 446, 429
Pratt, G. W., Arnaud, M., Piffaretti, R., et al. 2010, A&A, 511, A85
Predehl, P., Andritschke, R., Böhringer, H., et al. 2010, in Society of Photo-Optical Instrumentation Engineers (SPIE) Conference Series, Space Telescopes and Instrumentation 2010: Ultraviolet to Gamma Ray, eds. M. Arnaud, S. S. Murray, & T. Takahashi, 7732, 77320U
Reiprich, T. H., Hudson, D. S., Zhang, Y.-Y., et al. 2009, A&A, 501, 899
Rephaeli, Y., & Gruber, D. 2002, ApJ, 579, 587
Rephaeli, Y., Nevalainen, J., Ohashi, T., & Bykov, A. M. 2008, Space Sci. Rev., 134, 71
Rossetti, M., Eckert, D., Cavalleri, B. M., et al. 2011, A&A, 532, A123
Rybicki, G. B., & Lightman, A. P. 1985, Radiative processes in astrophysics, eds. George B. Rybicki, & Alan P. Lightman, 400. ISBN 0-471-82759-2 (Wiley-VCH), June 1986
Sanders, J. S., Fabian, A. C., & Smith, R. K. 2011, MNRAS, 410, 1797
Santos, J. S., Rosati, P., Tozzi, P., et al. 2008, A&A, 483, 35
Sarazin, C. L. 1988, X-ray emission from clusters of galaxies (Cambridge: Cambridge Univ. Press), 1988
Sato, K., Matsushita, K., Ishisaki, Y., et al. 2008, PASJ, 60, 333
Sato, T., Matsushita, K., Ota, N., et al. 2011, PASJ, 63, 991
Sato, T., Sasaki, T., Matsushita, K., et al. 2012, arXiv:1203.1700
Schuecker, P., Finoguenov, A., Miniati, F., Böhringer, H., & Briel, U. G. 2004, A&A, 426, 387
Simionescu, A., Allen, S. W., Mantz, A., et al. 2011, Science, 331, 1576
Smith, R. K., Brickhouse, N. S., Liedahl, D. A., & Raymond, J. C. 2001, ApJ, 556, L91
Sugawara, C., Takizawa, M., & Nakazawa, K. 2009, PASJ, 61, 1293
Sunyaev, R. A., Norman, M. L., & Bryan, G. L. 2003, Astronomy Letters, 29, 783
Suto, Y., Sasaki, S., & Makino, N. 1998, ApJ, 509, 544
Takahashi, T., Abe, K., Endo, M., et al. 2007, PASJ, 59, 35
Takahashi, T., Mitsuda, K., Kelley, R., et al. 2010, in Society of Photo-Optical Instrumentation Engineers (SPIE) Conference Series, Space Telescopes and Instrumentation 2010: Ultraviolet to Gamma Ray, eds. M. Arnaud, S. S. Murray, & T. Takahashi, 7732, 77320Z
Takizawa, M. 1999, ApJ, 520, 514
Tamura, T., Kaastra, J. S., Peterson, J. R., et al. 2001, A&A, 365, L87
Tamura, T., Hayashida, K., Ueda, S., & Nagai, M. 2011, PASJ, 63, 1009
Tozzi, P., & Norman, C. 2001, ApJ, 546, 63
Tyson, J. A., Kochanski, G. P., & dell'Antonio, I. P. 1998, ApJ, 498, L107
van Paradijs, J., & Bleeker, J. A. M., eds. 1999, X-Ray Spectroscopy in Astrophysics, Lecture Notes in Physics (Berlin: Springer Verlag), 520
Vikhlinin, A., Kravtsov, A., Forman, W., et al. 2006, ApJ, 640, 691
Voit, G. M. 2005, Reviews of Modern Physics, 77, 207
Wik, D. R., Sarazin, C. L., Finoguenov, A., et al. 2009, ApJ, 696, 1700
Wik, D. R., Sarazin, C. L., Finoguenov, A., et al. 2011, ApJ, 727, 119
Zhang, Y.-Y., Böhringer, H., Mellier, Y., Soucail, G., & Forman, W. 2005, A&A, 429, 85
Zu Hone, J. A., Lamb, D. Q., & Ricker, P. M. 2009, ApJ, 696, 694